

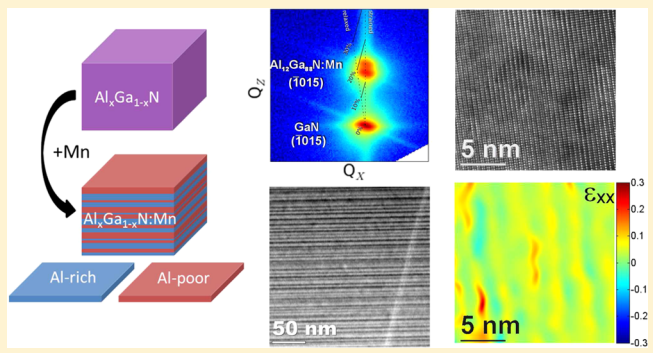
# Mn as Surfactant for the Self-Assembling of $\text{Al}_x\text{Ga}_{1-x}\text{N}/\text{GaN}$ Layered Heterostructures

Thibaut Devillers,\*† Li Tian,‡ Rajdeep Adhikari,† Giulia Capuzzo,† and Alberta Bonanni\*,†

†Institut für Halbleiter-und-Festkörperphysik, Johannes Kepler University, Altenbergerstr. 69, A-4040 Linz, Austria

‡Institute of Physics PAS SL 1.4, al. Lotników 32/46, 02-668 Warsaw, Poland

**ABSTRACT:** The structural analysis of GaN and  $\text{Al}_x\text{Ga}_{1-x}\text{N}/\text{GaN}$  heterostructures grown by metalorganic vapor phase epitaxy in the presence of Mn reveals how Mn affects the growth process and in particular, the incorporation of Al, the morphology of the surface, and the plastic relaxation of  $\text{Al}_x\text{Ga}_{1-x}\text{N}$  on GaN. Moreover, the doping with Mn promotes the formation of layered  $\text{Al}_x\text{Ga}_{1-x}\text{N}/\text{GaN}$  superlattice-like heterostructures, which opens wide perspectives for controlling the segregation of ternary alloys during the crystal growth and for fostering the self-assembling of functional layered structures.



## INTRODUCTION

Nitride heterostructures<sup>1</sup> are the building blocks of many state-of-the-art devices like power transistors,<sup>2</sup> high-electron-mobility transistors,<sup>3</sup> blue and white light-emitting diodes (LED),<sup>4</sup> ultraviolet laser diodes,<sup>5</sup> and blue lasers.<sup>6</sup> To produce a heterostructure whose band structure responds to the actual need, various combinations of nitride compounds with different band gaps and lattice parameters are epitaxially stacked to generate, for example, quantum wells,<sup>7</sup> superlattices, barriers,<sup>8</sup> or distributed Bragg reflector.<sup>9</sup> In any of these structures, the quality and continuity of the crystal is essential for the performance of the device. However, as expected during the epitaxial growth of lattice mismatched semiconductors, active layers of  $\text{Al}_x\text{Ga}_{1-x}\text{N}$  or  $\text{In}_x\text{Ga}_{1-x}\text{N}$ <sup>10</sup> deposited on GaN as requested by the architecture of most devices will tend to crack in order to relax the elastic strain accumulated by fitting the in-plane lattice parameter of the overlayer to the one of the layer underneath. Growing above the critical thickness is a challenging way to design high-performance devices with, for example, enhanced internal fields<sup>11,12</sup> and piezoelectric polarization.<sup>13</sup> In this perspective, the properties of the sample surface may be affected through the use of a surfactant.<sup>14</sup> The efficiency of this approach was already demonstrated in the case of Te for the growth of InAs on GaAs,<sup>15</sup> and As or Sb for Ge on Si.<sup>16</sup> Specifically, in the nitride technology, In,<sup>17–20</sup> As,<sup>21</sup> Ga,<sup>22</sup> and Sb<sup>23,24</sup> were reported to have a beneficial effect on the growth of GaN as well as on the fabrication of AlN/GaN heterostructures.

Here, we report on the role of Mn in the crystal growth of GaN:Mn and  $\text{Al}_x\text{Ga}_{1-x}\text{N}:\text{Mn}$  on GaN by metalorganic vapor phase epitaxy (MOVPE). In particular, we investigate how Mn affects both the morphology of the surface and the bulk crystal structure.

## EXPERIMENTAL SECTION

The studied samples are grown by MOVPE, in an AIXTRON 200RF horizontal reactor, according to a procedure described elsewhere.<sup>25</sup> A 1  $\mu\text{m}$  GaN buffer layer is deposited epitaxially at 1040 °C on sapphire *c*-plane after the growth of a low-temperature nucleation layer. The layers studied in this work are then deposited at a temperature of 850 °C on the GaN buffer. This unusually low growth temperature is of technical significance for several reasons. High growth temperatures (~1000 °C) on one hand promote the crystalline quality, but on the other favor the propagation of threading dislocations through the epitaxial films. Lower growth temperature, as employed in this work for the growth of (AlGa)N, hinders the propagation of the dislocations.<sup>26</sup> Furthermore, the difference in thermal expansion coefficient between overlayer and substrates may highly strain the layers during the cooling and induce cracking of the epitaxial structure. Thermal stress can be reduced significantly by using low growth temperatures. Finally, the integration of nitride technology in devices may require lower growth temperature to avoid the potentially detrimental diffusion of species during processing. The precursors employed for Ga, N, Al, and Mn are trimethylgallium (TMGa), ammonia ( $\text{NH}_3$ ), trimethylaluminum (TMAI), and bis-methylcyclopentadienyl-manganese ( $\text{MeCp}_2\text{Mn}$ ), respectively. The flow of TMGa and  $\text{NH}_3$  are fixed at 4  $\mu\text{mol}/\text{min}$  (1 sccm at 0 °C and 1000 mbar) and 7000  $\mu\text{mol}/\text{min}$ , respectively. The flow of  $\text{MeCp}_2\text{Mn}$  is roughly estimated to be in the order of 1  $\mu\text{mol}/\text{min}$  (490 sccm at 22 °C and 1000 mbar). The flow of TMAI is varied between 0.4 and 31  $\mu\text{mol}/\text{min}$ . The growth is carried out under  $\text{H}_2$  atmosphere at a pressure of 100 mbar for the  $\text{Al}_x\text{Ga}_{1-x}\text{N}$  ( $\text{Al}_x\text{Ga}_{1-x}\text{N}:\text{Mn}$ ) layers and 200 mbar for the GaN (GaN:Mn). The relevant characteristics of the samples studied here are summarized in Table 1. The thickness of the layers is controlled *in situ* during the growth process by kinetic ellipsometry and *ex situ* with spectroscopic ellipsometry, secondary ion mass

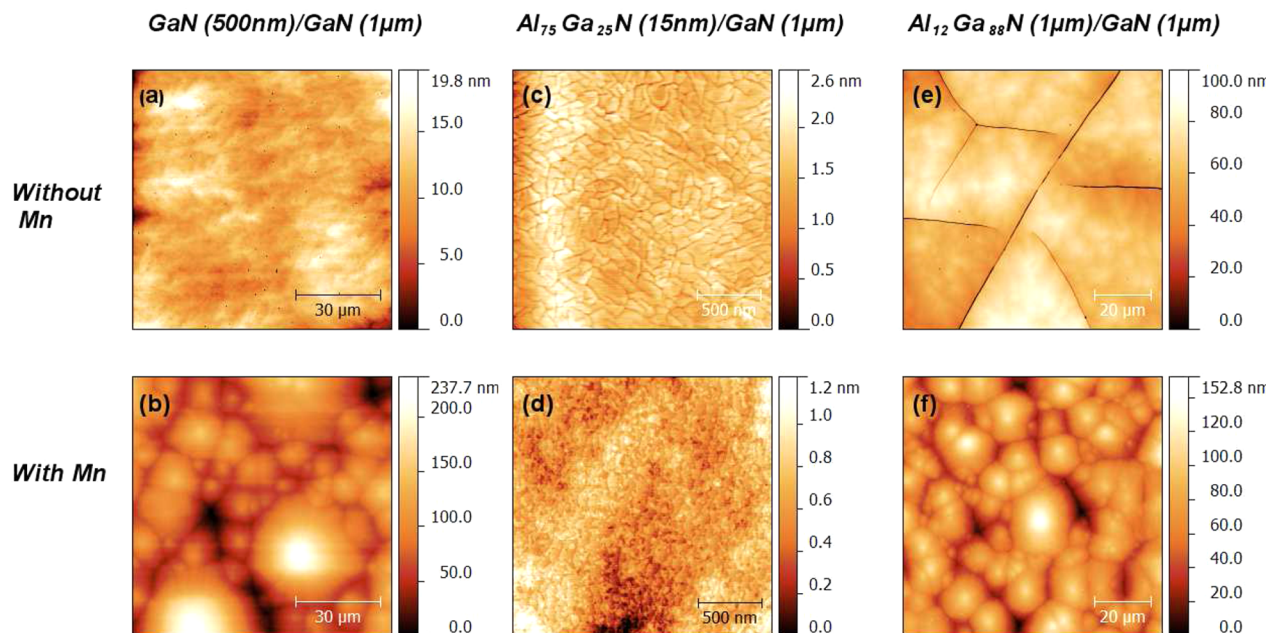
Received: July 30, 2014

Revised: December 11, 2014

Published: January 8, 2015

Table 1. Samples Investigated and Their Relevant Parameters

sample	buffer	layer	thickness (nm)	Al concentration (%)	growth temperature (°C)	growth pressure (mbar)
#A	GaN	GaN	500	0	850	200
#B	GaN	GaN:Mn	500	0	850	200
#C	GaN	AlGaN	15	75	850	100
#D	GaN	AlGaN:Mn	15	75	850	100
#E	GaN	AlGaN	1000	12	850	100
#F	GaN	AlGaN:Mn	1000	12	850	100

Figure 1. Atomic force micrographs for: (a, c, e) GaN and  $\text{Al}_x\text{Ga}_{1-x}\text{N}$  in the absence of Mn; (b, d, f) GaN:Mn and  $\text{Al}_x\text{Ga}_{1-x}\text{N}:\text{Mn}$ .

spectroscopy (SIMS), and X-ray reflectivity. The Al concentration is calculated from the position of the (0002) and ( $\bar{1}015$ ) diffraction peaks of  $\text{Al}_x\text{Ga}_{1-x}\text{N}$ .

Information on the morphology of the surface is obtained from atomic force microscopy (AFM) in tapping mode with a Nanosurf MobileS and with a VEECO Dimension 3100. X-ray diffraction (XRD) and reflectivity are performed on a PANalytical's X'Pert PRO Materials Research Diffractometer (MRD) equipped with a hybrid monochromator with a  $1/4^\circ$  divergence slit. The diffracted beam is measured with a solid-state PixCel detector used as 256-channel detector with a 11.9 mm antiscatter slit. Transmission electron microscopy (TEM) in both conventional (CTEM) and scanning mode (STEM) is performed in a FEI Titan Cube 80–300 operating at 300 keV and in a JEOL 2010F working at 200 keV. Bright/dark-field (BF/DF), high-resolution TEM (HRTEM), and high-angle annular dark field (HAADF) are employed to analyze the structure of the sample. Chemical mapping is performed with energy filtered TEM (EFTEM) around the Al K absorption edge. Cross-section TEM specimens are prepared by mechanical polishing, dimpling, and final ion milling in a Gatan Precision Ion Polishing System.

## RESULTS AND DISCUSSION

The effect of Mn on the surface morphology of GaN and  $\text{Al}_x\text{Ga}_{1-x}\text{N}$  is studied by AFM by directly contrasting GaN,  $\text{Al}_{0.75}\text{Ga}_{0.25}\text{N}$  and  $\text{Al}_{0.12}\text{Ga}_{0.88}\text{N}$  grown in the absence of Mn (samples #A, #C, and #E) with samples grown under the same conditions but deposited in the presence of Mn (samples #B, #D, and #F), as reported in Figure 1. The compared samples have the same nominal and actual thickness and differ only in the presence of Mn during the growth process.

As evidenced in Figure 1, panels (a) and (b), the addition of Mn during the growth of GaN at  $T_G = 850$  °C affects the morphology of the surface by inducing the formation of large domes. This effect resembles the one observed by Zhang et al.<sup>24</sup> during the growth of GaN in the presence of antimony (Sb), where Sb was found to act as a surfactant during the growth, promoting the mobility of Ga atoms on the surface, and thus lateral growth. In our case, the fact that Mn plays the role of a surfactant is coherent with its low probability of incorporation into the crystal. Despite the relatively high flow rate of the  $\text{MeCp}_2\text{Mn}$  precursor during the epitaxial process (20% of the III metal precursor flow), the Mn content in the layers remains in the order of 1% cations as established through SIMS measurements, which show that a large part of the Mn is not incorporated in the layer and is either desorbed or accumulated at the surface. The dramatic effect that we do observe on the growth and particularly at the surface rather suggests that an important part of the Mn atoms accumulates at the growth front and influences the dynamics of epitaxy. In addition to the presence of domes in the samples grown in the presence of Mn, there is no hint of linear (cracks) or punctual (pits) discontinuities of the layers, and one can still distinguish in higher resolution images (not shown) the atomic terrace edges characteristic of a step-flow growth mode. Furthermore, despite the waviness of the surface and since it was already demonstrated in the case of Mn-doped GaN (ref 25), the Mn does not affect the single-crystalline character of the layers since it also does not significantly affect the dislocation density in the films compared to the GaN buffer layer. In Figure 1,

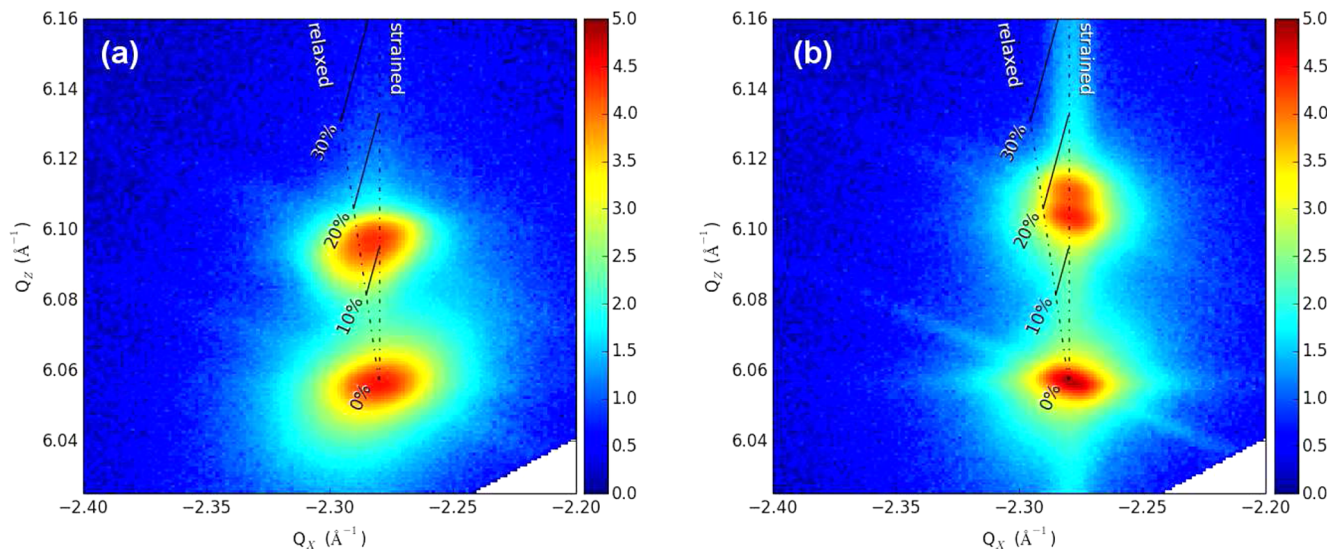


**Figure 2.** Reciprocal space maps around GaN and  $\text{Al}_x\text{Ga}_{1-x}\text{N}(\bar{1}015)$  for: (a) sample #E and (b) sample #F. The intensity is reported in logarithmic scale. A vertical dashed line along the GaN ( $\bar{1}01$ ) and an oblique dashed line joining experimental GaN and AlN ( $\bar{1}015$ ) are drawn as guides to the eye. The isoconcentration lines are indicated as continuous lines between the strained and relaxed states.

panels (c) and (d), the effect of Mn on the growth of 15 nm thin  $\text{Al}_{0.75}\text{Ga}_{0.25}\text{N}$  layers is evidenced. In the Mn-free layer, the expected morphology of  $\text{Al}_x\text{Ga}_{1-x}\text{N}$  close to relaxation<sup>27</sup> can be appreciated: shallow fractures—precursors of the cracks observed for relaxed thicker layers—are detected. Both samples are grown under the same conditions, which resulted in the same thickness (as determined from the fitting of X-ray reflectivity) and same Al content (as obtained from the position of the ( $\bar{1}015$ ) asymmetric peak and from fitting the X-ray reflectivity). The layer grown in the presence of Mn, even if the thickness and the Al concentration are kept constant, exhibits a surface free of nanofractures, which points to the fact that Mn delays the relaxation of the lattice like Sb in the case of Ge grown on Si,<sup>16</sup> or Te in InAs on GaAs.<sup>15</sup>

For a closer analysis of the role of Mn in the relaxation of  $\text{Al}_x\text{Ga}_{1-x}\text{N}$  on GaN, two layers of  $\text{Al}_{0.12}\text{Ga}_{0.88}\text{N}$ , with and without Mn respectively, and with a thickness of 1  $\mu\text{m}$ , that is, theoretically above the critical thickness,<sup>28</sup> are compared. The  $\text{Al}_{0.12}\text{Ga}_{0.88}\text{N}$  layer grown without Mn and shown in Figure 1, panel e presents surface grooves oriented at either 60° or 120° one with respect to the other. These cracks are characteristic of the heteroepitaxy of  $\text{Al}_x\text{Ga}_{1-x}\text{N}$  on GaN above the critical thickness and can already be observed in a sample twice thinner and grown under the same conditions (not shown). In contrast, in the presence of Mn (sample #F), the domes already seen in GaN:Mn are detected, but there is no evidence of cracks in the field of view, as shown in Figure 1, panel (f). The incorporation of Mn in the  $\text{Al}_x\text{Ga}_{1-x}\text{N}$  layers also seems to have a beneficial effect on the defect density of  $\text{Al}_x\text{Ga}_{1-x}\text{N}$  grown at 850 °C since the presence of Mn induces the annihilation of the yellow luminescence, which is characteristic of deep acceptors defects in nitrides semiconductors (not shown here). Optical microscopy in reflection mode also reveals the presence of cracks in the Mn-free sample, while a whole 2 inches wafer grown in the presence of Mn is completely crack-free, which points to an  $\text{Al}_x\text{Ga}_{1-x}\text{N}$  layer perfectly strained with the GaN buffer.

This result is confirmed by XRD experiments. Reciprocal space maps have been measured around the ( $\bar{1}015$ ) reflection of GaN and  $\text{Al}_x\text{Ga}_{1-x}\text{N}$  and are reported in Figure 2 for samples

#E and #F. The shape and position of this peak appear to be different for the two samples: the center of the peak is shifted toward lower in-plane lattice parameters in the case of the Mn-free sample. Here, the average lattice parameter of the layer does not fit the one of GaN, which indicates a plastic relaxation of the crystal lattice. In fact, the peak is neither aligned with the dashed line, which corresponds to a fully relaxed layer, nor with the one corresponding to a fully strained state, which points to an intermediate strain state. Furthermore, the peak is particularly broad and actually spreads over the whole range between strained and relaxed state. In comparison, in the presence of Mn, the ( $\bar{1}015$ ) reflection of AlGaN is very narrow in  $Q_x$  and vertically aligned with the ( $\bar{1}015$ ) of GaN, which confirms the strained state of the layer already evidenced by surface microscopy. The Al concentration is comparable in the two samples; the peak of the layer containing Mn and not relaxed is shifted toward higher values of  $Q_z$  due to the limited compressibility of the material. In addition, this peak exhibits an unexpected broadening along the  $Q_z$  direction, which suggests the presence of  $\text{Al}_x\text{Ga}_{1-x}\text{N}$  with different Al concentrations. To quantify the Al content in the films from the position of the ( $\bar{1}015$ ) peak, we assume a linear variation of the out-of-plane lattice parameter with the Al content in the whole range of concentrations from GaN to AlN (Vegard's law). In the completely relaxed case, the Al concentration is given by  $x_{\text{Al}} = ((c_{\text{AlGaN}} - c_{\text{GaN}})/(c_{\text{AlN}} - c_{\text{GaN}}))$ . In the perfectly strained case, it is necessary to add a prefactor to take into account the elongation of the lattice along the  $c$  direction when the crystal is elongated along the  $a$ -axis. The Al concentration is then obtained through  $x_{\text{Al}} = ((1 - \nu)/(1 + \nu)(c_{\text{AlGaN}} - c_{\text{GaN}})/(c_{\text{AlN}} - c_{\text{GaN}}))$ , where  $\nu$  is the Poisson coefficient (0.19 and 0.21 for GaN and AlN respectively<sup>1</sup>). The calculated Al concentration is thus in the considered sample ( $12 \pm 1\%$ ) for the partially relaxed Mn-free layer (sample #E). For the Mn-containing layer (sample #F), the two main peaks related to  $\text{Al}_x\text{Ga}_{1-x}\text{N}$  correspond to Al contents of 12.8% and 14.3%, respectively.

To shed light on the origin of the different Al concentrations detected by XRD in the films doped with Mn, the nature of the Al inhomogeneity and the role of Mn on the Al segregation have been investigated with HRTEM. In Figure 3, panel (a), a

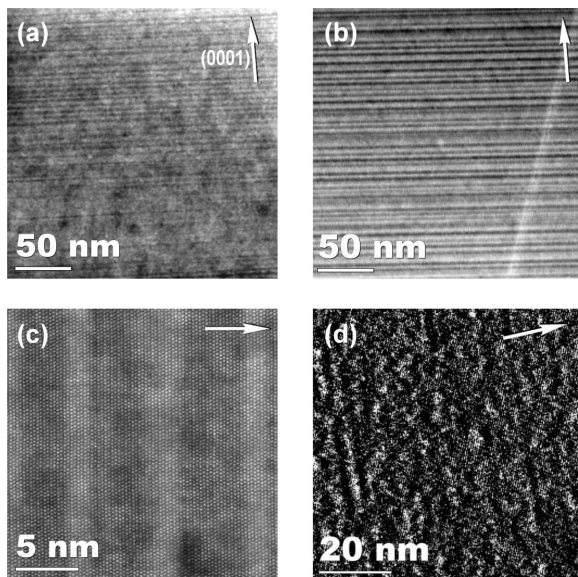


**Figure 3.** TEM of the  $\text{Al}_x\text{Ga}_{1-x}\text{N}:\text{Mn}$  layer of sample #F in cross-section measured along the  $[1\bar{1}20]$  zone axis: (a) low magnification conventional TEM; (b) low magnification HAADF; (c) high resolution HAADF; (d) Al chemical map from energy filtered TEM measured at Al K-edge; in all panels, the  $(0001)$  direction is indicated by an arrow.

low magnification transmission electron micrograph of the  $\text{Al}_{0.12}\text{Ga}_{0.88}\text{N}:\text{Mn}$  layer reveals along the  $c$ -axis the presence of a quasi-periodic structure, which is not observed in the Mn-free samples. An analysis of over 40 sublayers gives an average thickness of 2.9 nm with a standard deviation of 0.73 nm. No significant difference in the thickness of darker and brighter layers could be found. Both in TEM and in XRD, the nonperfect periodicity of the superlattice does not allow to resolve the satellite peaks characteristic of a superlattice. To discriminate between the contrast due to diffraction effects from the one induced by composition contrast, the same layer has been measured in HAADF in STEM mode. Within this imaging technique, electron diffusion measured at a high angle is decisively dependent on the mass of the diffusing elements. The contrast observed can therefore be directly correlated with a mass contrast, the Al-rich areas being darker than the Ga-rich ones. The HAADF measurements are reported in Figure 3, panels (b) and (c) and show a similar patterning as in Figure 3, panel (a). This suggests that the contrast observed in

conventional TEM is induced by a modulation in the Al concentration. This result is also confirmed by the energy filtered image displayed in Figure 3, panel (d). This image has been acquired in EFTEM around the Al K-edge, and the bright areas correspond to Al-rich regions. This element-specific technique confirms that the mass contrast observed in HAADF originates indeed from Al segregation and not only from a variation of the density of the material, which could be eventually induced by the presence of defects.

A similar self-structuring of ternary alloys in superlattice-like heterostructures was already reported for the growth of  $\text{Al}_x\text{Ga}_{1-x}\text{N}$  on GaN (refs 29, 30) and AlN (refs 31–34). Particularly remarkable here is not the segregation of Al itself but rather the fact that we are able to trigger the segregation and the self-assembling of layered structures through the presence of Mn. To figure out the underlying mechanism, one should consider that Mn is here playing the role of an efficient surfactant and is mostly accumulating at the growing surface. Therefore, Mn behaves like the cations Ga and Al and affects radically the equilibrium between the metal (Al or Ga) and nitrogen, that is, the III/V ratio, which is known to have a key role in the decomposition into superlattices.<sup>31,33</sup>

Since the layer (sample #F) is pseudomorphically grown on GaN, the modulation of the Al concentration is expected to be accompanied by a modulation of the  $c$ -parameter. To establish the strain distribution in the layer, a geometrical phase analysis (GPA) according to the technique developed by Hjøtch et al.<sup>35</sup> has been performed. The GPA is implemented from the high resolution micrograph measured in the  $[11\bar{2}0]$  zone axis and reported in Figure 4, panel (a). Since the phase modulation takes place in the whole area of imaging and since the strain state in this area is a priori unknown, the average phase must be taken as a reference for the calculation of the strain. The strain maps are calculated along the  $c$ - and  $a$ -axes and represented in Figure 4, panels (b) and (c), respectively.

The absence of strain contrast along the  $a$ -direction is coherent with the pseudomorphic character of the layer already evidenced by XRD. The quasi-periodic structure detectable in the strain map calculated along the  $c$ -direction indicates that the  $c$  lattice parameter is modulated, which confirms the periodic variation of Al content already observed in HAADF. The average lattice parameter measured in the HRTEM considered in Figure 4, panel (a) is 5.128 Å, which by taking into account the strained character of the layer, corresponds to an Al concentration of 13.1%. The average negative strain (compressive) and positive strain (tensile) in Figure 4, panel (b) are

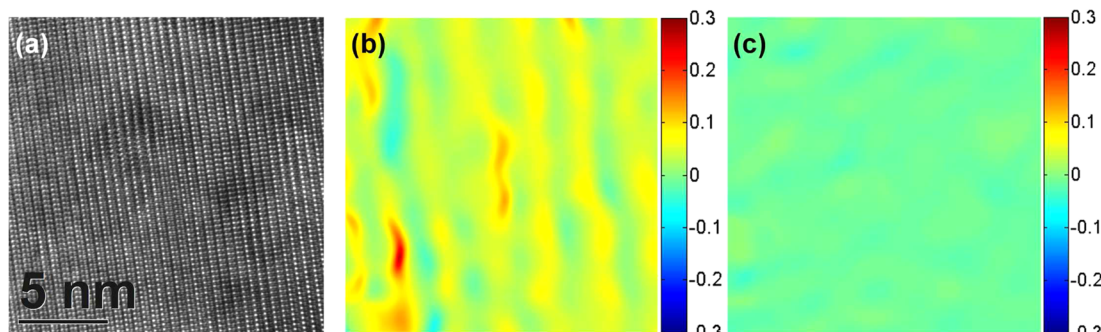


**Figure 4.** Strain analysis for  $\text{Al}_{0.12}\text{Ga}_{0.88}\text{N}:\text{Mn}$  (sample #F) obtained through the geometrical phase analysis method:<sup>35</sup> (a) high-resolution transmission electron micrograph in cross-section taken along  $[11\bar{2}0]$  zone axis; (b, c) corresponding strain maps along the  $c$ - and  $a$ -direction, respectively.

–1.94% and 2.84% and correspond to a *c*-parameter of 5.029 and 5.274 Å, respectively. Considering that the layer is pseudomorphically grown on GaN, a *c*-parameter of 5.029 Å gives an Al concentration of about 35.0%, which is far above the one extracted from XRD, while 5.274 Å is greater than the *c*-parameter of relaxed GaN (5.185 Å). This unexpectedly large lattice parameter can be explained by the presence of local defects that locally distort the lattice. On the other hand, it must be considered that the nonperfect periodicity of the layered structure is likely to generate a broad diffraction line containing  $\text{Al}_x\text{Ga}_{1-x}\text{N}$  and GaN peaks, rather than well-defined satellites, as evidenced in Figure 2, panel (b). A similar weak effect can be also appreciated in the fast Fourier transform (FFT) of some of the HRTEM pictures, particularly in two beam condition, where the (0002) peak gets elongated in the (0001) direction. Such a pattern in the FFT of Figure 4, panel (a), and particularly the fact that a part of it may get lost in selecting the diffracted spot used for the strain calculation, may produce a systematic error in the quantification of the strain and consequently of the lattice parameter. This error could give too high (respectively low) lattice parameter for low (respectively high) Al content layers in the superlattice.

## CONCLUSIONS

We have shown that Mn acts as a surfactant in the MOVPE of the technologically strategic compounds GaN and  $\text{Al}_x\text{Ga}_{1-x}\text{N}$  and affects the surface morphology and the crystalline arrangement. Most remarkably, in the case of low Al concentrations, we have found that Mn induces the segregation of Al in the  $\text{Al}_x\text{Ga}_{1-x}\text{N}:\text{Mn}$  films and promotes the self-assembling of layered superlattice-like structures. In a larger perspective and particularly in the case of reactive crystal growth techniques, among which MOVPE, the use of appropriate surfactants, and their potential of affecting the balance between the different species involved in the growth process, can open a new route to control the segregation of selected elements in ternary and more complex alloys and to promote the self-assembling of functional heterostructures.

## AUTHOR INFORMATION

### Corresponding Authors

\*E-mail: thibaut.devillers@neel.cnrs.fr.

\*E-mail: alberta.bonanni@jku.at.

### Notes

The authors declare no competing financial interest.

## ACKNOWLEDGMENTS

This work was supported by the European Research Council (ERC Advanced Grant 227690), the Austrian Science Fundation (FWF Projects 22477, 24471), and WRC EIT+ within the project NanoMat (P2IG.01.01.02-02-002/08) cofinanced by the European Operational Programme Innovative Economy (1.1.2).

## REFERENCES

- (1) Morkoç, H. *Handbook of Nitride Semiconductors*; Wiley-VCH Verlag GmbH: Weinheim, Germany, 2008; Vol. 3.
- (2) Shur, M. *Solid-State Electron.* **1998**, *42*, 2131–2138.
- (3) Mishra, U. K. *Proc. IEEE* **2002**, *90*, 1022–1031.
- (4) Gutt, R.; Passow, T.; Kunzer, M.; Pletschen, W.; Kirste, L.; Forghani, K.; Scholz, F.; Köller, K.; Wagner, J. *Appl. Phys. Express* **2012**, *5*, 32101–32103.

- (5) Yoshida, H.; Yamashita, Y.; Kuwabara, M.; Kan, H. *Nat. Photonics* **2008**, *2*, 551–554.
- (6) Nakamura, S.; Chichibu, S. F. *Introduction to Nitride Semiconductor Blue Lasers and Light Emitting Diodes*; CRC Press: Boca Raton, FL, 2000.
- (7) Lepkowski, S.; Gorczyca, I.; Stefanska-Skrobas, K.; Christensen, N.; Svane, A. *Phys. Rev. B* **2013**, *88*, 081202(R).
- (8) Manuel, J.; Morales, F.; Garcia, R.; Lim, T.; Kirste, L.; Aidam, R.; Ambacher, O. *Cryst. Growth Des.* **2011**, *11*, 2588–2591.
- (9) Kruse, C.; Dartsch, H.; Aschenbrenner, T.; Figge, S.; Hommel, D. *Phys. Status Solidi B* **2011**, *248*, 1748–1755.
- (10) Ra, Y.-H.; Navamathavan, R.; Park, J.-H.; Lee, C.-R. *ACS Appl. Mater. Interfaces* **2013**, *5*, 2111–2117.
- (11) Songmuang, R.; Kalita, D.; den Hertog, M.; Andre, R.; Ben, T.; Gonzalez, D.; Mariette, H.; Monroy, E. *Appl. Phys. Lett.* **2011**, *99*, 141914.
- (12) Dong, P.; Jan, Y.; Zhang, Y.; Wang, J.; Geng, C.; Theng, H.; Wei, X.; Yan, Q.; Li, J. *Opt. Express* **2014**, *22*, A320–A327.
- (13) Ambacher, O.; Foutz, B.; Smart, J.; Shealy, J.; Weimann, N.; Chu, K.; Murphy, M.; Sierakowski, A.; Shaff, W.; Eastmann, L.; Dimitrov, R.; Mitchell, A.; Stutzmann, M. *J. Appl. Phys.* **2000**, *87*, 334.
- (14) Copel, M.; Reuter, M. C.; Kaxiras, E.; Tromp, R. M. *Phys. Rev. Lett.* **1989**, *63*, 632–635.
- (15) Grandjean, N.; Massies, J.; Etgens, V. H. *Phys. Rev. Lett.* **1992**, *69*, 796–799.
- (16) Osten, H. J.; Lippert, G.; Klatt, J. *J. Vac. Sci. Technol., B* **1992**, *10*, 1151–1155.
- (17) Widmann, F.; Daudin, B.; Feuillet, G.; Pelekanos, N.; Rouvière, J. L. *Appl. Phys. Lett.* **1998**, *73*, 2642–2644.
- (18) Keller, S.; Heikman, S.; Ben-yaacov, I.; Shen, L.; DenBaars, S.; Mishra, U. *Phys. Status Solidi A* **2001**, *188*, 775–778.
- (19) Monroy, E.; Daudin, B.; Gogneau, N.; Bellet-Amalric, E.; Jalabert, D.; Brault, J. *Phys. Status Solidi B* **2002**, *234*, 726–729.
- (20) Nicolay, S.; Feltin, E.; Carlin, J.-F.; Mosca, M.; Nevou, L.; Tchernycheva, M.; Julien, F.-H.; Ilgemes, M.; Grandjean, N. *Appl. Phys. Lett.* **2006**, *88*, 151902.
- (21) Okumura, H.; Hamaguchi, H.; Feuillet, G.; Ishida, Y.; Yoshida, S. *Appl. Phys. Lett.* **1998**, *72*, 3056–3058.
- (22) Mula, G.; Adelmann, C.; Moehl, S.; Oullier, J.; Daudin, B. *Phys. Rev. B* **2001**, *64*, 195406.
- (23) Zhang, L.; Tang, H. F.; Kuech, T. F. *Appl. Phys. Lett.* **2001**, *79*, 3059–3061.
- (24) Zhang, L.; Tang, H.; Schieke, J.; Mavrikakis, M.; Kuech, T. J. *Cryst. Growth* **2002**, *242*, 302–308.
- (25) Stefanowicz, W.; Sztenkiel, D.; Faina, B.; Grois, A.; Rovezzi, M.; Devillers, T.; d’Acapito, F.; Navarro-Quezada, A.; Li, T.; Jakielka, R.; Sawicki, M.; Dietl, T.; Bonanni, A. *Phys. Rev. B* **2010**, *81*, 235210.
- (26) Bourret-Courchesne, E. D.; Kellermann, S.; Yu, K. M.; Benamara, M.; Liliental-Weber, Z.; Washburn, J.; Irvine, S. J. C.; Stafford, A. *Appl. Phys. Lett.* **2000**, *77*, 3562–3564.
- (27) Keller, S.; Parish, G.; Fini, P. T.; Heikman, S.; Chen, C.-H.; Zhang, N.; DenBaars, S. P.; Mishra, U. K.; Wu, Y.-F. *J. Appl. Phys.* **1999**, *86*, 5850–5857.
- (28) Lee, S. R.; Koleske, D. D.; Cross, K. C.; Floro, J. A.; Waldrip, K. E.; Wise, A. T.; Mahajan, S. *Appl. Phys. Lett.* **2004**, *85*, 6164–6166.
- (29) Korakakis, D.; Ludwig, K. F.; Moustakas, T. D. *Appl. Phys. Lett.* **1997**, *71*, 72–74.
- (30) Doppalapudi, D.; Basu, S. N.; Ludwig, K. F.; Moustakas, T. D. *J. Appl. Phys.* **1998**, *84*, 1389–1395.
- (31) Iliopoulos, E.; Ludwig, K. F.; Moustakas, T. D.; Chu, S. N. G. *Appl. Phys. Lett.* **2001**, *78*, 463–465.
- (32) Gao, M.; Bradley, S. T.; Cao, Y.; Jena, D.; Lin, Y.; Ringel, S. A.; Hwang, J.; Schaff, W. J.; Brillson, L. J. *J. Appl. Phys.* **2006**, *100*, 103512.
- (33) Wang, Y.; Özcan, A. S.; Ludwig, K. F.; Bhattacharyya, A.; Moustakas, T. D.; Zhou, L.; Smith, D. J. *Appl. Phys. Lett.* **2006**, *88*, 181915.
- (34) Kim, H.; Choi, S.; Yoo, D.; Ryou, J.-H.; Hawkridge, M.; Liliental-Weber, Z.; Dupuis, R. *J. Electron. Mater.* **2010**, *39*, 466–472.

(35) Hjøtch, M.; Snoeck, E.; Kilaas, R. *Ultramicroscopy* **1998**, *74*, 131–146.